Terahertz and infrared photodetection using p-i-n multiple-graphene-layer structures

doi: 10.1063/1.3327441

Terahertz and infrared photodetection using p-i-n multiple-graphene-layer structures

V. Ryzhii,[1,2,a)] M. Ryzhii,[1,2] V. Mitin,[3] and T. Otsuji[2,4]
[1]*Computational Nanoelectronics Laboratory, University of Aizu, Aizu-Wakamatsu 965-8580, Japan*
[2]*Japan Science and Technology Agency, CREST, Tokyo 107-0075, Japan*
[3]*Department of Electrical Engineering, University at Buffalo, State University of New York, New York 14260, USA*
[4]*Research Institute for Electrical Communication, Tohoku University, Sendai 980-8577, Japan*

(Received 2 December 2009; accepted 26 January 2010; published online 9 March 2010)

We propose to utilize multiple-graphene-layer structures with lateral p-i-n junctions for terahertz and infrared (IR) photodetection and substantiate the operation of photodetectors based on these structures. Using the developed device model, we calculate the detector dc responsivity and detectivity as functions of the number of graphene layers and geometrical parameters and show that the dc responsivity and detectivity can be fairly large, particularly, at the lower end of the terahertz range at room temperatures. Due to relatively high quantum efficiency and low thermogeneration rate, the photodetectors under consideration can substantially surpass other terahertz and IR detectors. Calculations of the detector responsivity as a function of modulation frequency of THz and IR radiation demonstrate that the proposed photodetectors are very fast and can operate at the modulation frequency of several tens of gigahertz. © *2010 American Institute of Physics*. [doi:10.1063/1.3327441]

I. INTRODUCTION

Unique properties of graphene layers (GLs)[1–3] make them promising for different nanoelectronic device applications. The gapless energy spectrum of GLs, which is an obstacle for creating transistor-based digital circuits, opens up prospects to use GLs in terahertz and infrared (IR) devices. Novel optoelectronic terahertz and IR devices were proposed and evaluated, in particular, in Refs. 4–11. Recent success in fabricating multiple-GL structures with long momentum relaxation time of electrons and holes[12] promises a significant enhancement of the performance of future graphene optoelectronic devices.[13]

In this paper, we study the operation of terahertz and IR photodetectors based on multiple-GL structures with reverse biased p-i-n junctions. We refer to the photodetectors in question as to GL-photodetectors (GLPDs). We focus on GLPDs (a) with p- and n-doped sections in GLs near the side contacts,[14,15] p^+ and n^+ contacts (for example, made of doped poly-Si),[16] and multiple GL-structures with the Ohmic side contacts and (b) with split gates which provide the formation of the electrically induced p- and n-sections.[17–22] These gates are separated from a multiple-GL structure by a insulating layer (gate layer) made of, for instance, SiO_2 or HfO_2. Its thickness W_g should be chosen (sufficiently small) to provide an effective formation of the electron and hole regions under the gates in sufficiently large number of GLs under the applied gate voltages. The device structures under considerations are shown in Figs. 1(a) and 1(b). It is assumed that the highly conducting GL(s) between the SiC substrate and the top GLs is removed. Multiple GL-structures without this highly conducting GL can be fabricated using chemical/mechanical reactions and transferred substrate techniques (chemically etching the substrate and the highly conducting bottom GL (Ref. 23) or mechanically peeling the upper GLs, then transferring the upper portion of the multiple-GL structure on a Si substrate). The operation of GLPDs is associated with the interband photogeneration of the electrons and holes in the i-sections of GLs by incoming THz or IR radiation. The photogenerated electrons and holes propagate under the electric field created by the bias voltage (which provides the p-i-n junction reverse bias) in the directions toward the n-section and p-section, respectively. This results in the dc or ac photocurrent induced in the circuit. The GLPD operation principle is actually similar to that in the standard p-i-n photodiodes based on bulk semiconductor materials.

Using the developed device model, we calculate the GLPD responsivity and detectivity as terahertz or IR photodetector (Secs. II and III), evaluate its dynamic response

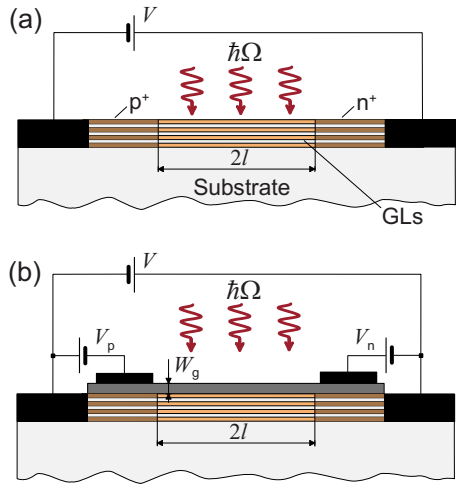

FIG. 1. (Color online) Device structures of GLPDs with (a) doped and (b) electrically induced p-i-n junctions.

a)Electronic mail: v-ryzhii@u-aizu.ac.jp.

(Sec. IV), and compare GLPDs with some other terahertz and IR photodetectors (Sec. V), in particular, with quantum-well IR photodetectors (QWIPs) and quantum-dot IR photodetectors (QDIPs). In Sec. VI, we discuss possible role of the Pauli blocking in the spectral characteristics of GLPDs and draw main conclusions. The calculations related to the effect of screening of the vertical electric field on the formation of the electrically induced p- and n-sections in multiple-GL structures are singled out in the Appendix.

II. RESPONSIVITY AND DETECTIVITY

We assume that the intensity of the incident terahertz or IR radiation with the frequency Ω apart from the dc component I_0 includes the ac component: $I(t)=I_0+\delta I_\omega \exp(-i\omega)t$, where δI_ω and ω are the amplitude of the latter component and its modulation frequency, respectively. In such a situation, the net dc current (per unit width of the device in the direction perpendicular to the current) can be presented in the following form:

$$J_0 = J_0^{\rm dark} + J_0^{\rm photo}, \tag{1}$$

with

$$J_0^{\rm dark} = 4Kel(g_{\rm th} + g_{\rm tunn}) \tag{2}$$

and

$$J_0^{\rm photo} = 4el\sum_{k=1}^{K} \frac{\beta_\Omega I_0^{(k)}}{\hbar\Omega}. \tag{3}$$

Here e is the electron charge, K is the number of GLs, $2l$ is the length of the GL i-section, $g_{\rm th}$ and $g_{\rm tunn}=(eV/2lv_W^{2/3}\hbar)^{3/2}/8\pi^2$ are the rates of thermal and tunneling generation of the electron-hole pairs (per unit area),[22] V is the reverse bias voltage, $v_W \simeq 10^8$ cm/s is the characteristic velocity of electrons and holes in graphene (see, for instance, Ref. 3), $\beta_\Omega=\beta[1-2f(\hbar\Omega/2)]$ is the absorption coefficient of radiation in a GL due to the interband transitions,[24] where $\beta=(\pi e^2/c\hbar)\simeq 0.023$, $f(\varepsilon)$ is the distribution function of electrons and holes in the i-section, $\hbar$ is the Planck constant, and c is the speed of light. The term $g_{\rm tunn}$ in Eq. (2) is associated with the interband tunneling in the electric field in the i-section. The quantity $I_0^{(k)}=I_0(1-\beta_\Omega)^{K-k}$ is the intensity of terahertz or IR radiation at the kth GL ($1\le k\le K$).

At a sufficiently strong reverse bias, electrons and holes are effectively swept out from the i-section to the contacts and heated. Due to this, one can assume that under the GLPD operation conditions, $f(\hbar\Omega/2)\ll 1$, so that the distinction between β_Ω and β can be disregarded (see below).

Using Eqs. (1) and (3), we arrive at the following formula for the GLPD dc responsivity:

$$R_0 = \frac{J_0^{\rm photo}}{2lI_0} = K^*\frac{2e\beta_\Omega}{\hbar\Omega}, \tag{4}$$

where $K^*=\Sigma_{k=1}^{K}(1-\beta_\Omega)^{K-k}=[1-(1-\beta_\Omega)^K]/\beta_\Omega$. Equation (4) can also be rewritten as

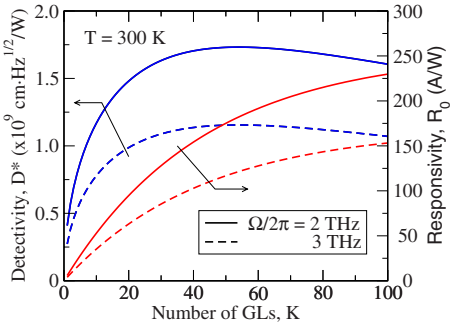

FIG. 2. (Color online) Responsivity R_0 and detectivity D^* vs number of GLs K for $\Omega/2\pi=2$ and 3 THz.

$$R_0 = [1-(1-\beta_\Omega)^K]\frac{2e}{\hbar\Omega} = \eta\frac{e}{\hbar\Omega} \propto \frac{1}{\hbar\Omega}, \tag{5}$$

where $\eta=2[1-(1-\beta_\Omega)^K]$ is the GLPD quantum efficiency and the factor 2 appears because each photon absorbed due to the interband transition generates two carriers, an electron and a hole. As a result, η can exceed unity. However, $\eta<2$ because there is no multiplication of the photoelectrons and photoholes propagating in the i-section, so that the photoelectric gain G in the photodetectors under consideration is equal (or, at least, close) to unity. If $K=1$, Eq. (5) at $\Omega/2\pi=1$ THz, yields, $R_0\simeq 12$ A/W. For $K=50-100$ ($K^*\simeq 30-39$), setting $K=50$, in the frequency range $\Omega/2\pi=1-10$ THz, from Eq. (4) we obtain $R_0\simeq 35-350$ A/W. As follows from Eqs. (4) and (5), the GLPD responsivity is virtually independent of the temperature. This results from the temperature-independent absorption coefficient and $G\simeq 1$.

The dark-current limited detectivity, D^*, defined as $D^*=(J^{\rm photo}/NP)\sqrt{A\cdot\Delta f}$, where N is the noise (in Amperes), P is the power received by the photodetector (in watts), A is the area of the photodetector (in cm^2) (see, for instance, Refs. 25 and 26), and Δf is the bandwidth, can be expressed via the responsivity R_0 and the dark current $J_0^{\rm dark}H$, where H is the device width in the direction perpendicular to the current, and be presented as

$$D^* = R_0\sqrt{\frac{A}{4eJ_0^{\rm dark}H}}. \tag{6}$$

Using Eqs. (2)–(6), we arrive at

$$D^* = \frac{K^*}{\sqrt{K}}\frac{\beta_\Omega}{\hbar\Omega}\frac{1}{\sqrt{2(g_{\rm th}+g_{\rm tunn})}} = \frac{[1-(1-\beta_\Omega)^K]}{\sqrt{K}\hbar\Omega}\frac{1}{\sqrt{2(g_{\rm th}+g_{\rm tunn})}} \propto \frac{1}{\hbar\Omega}. \tag{7}$$

Assuming that $K=1$ and $g_{\rm th}=10^{21}$ cm^{-2} s^{-1},[27] at $T=300$ K for $\Omega/2\pi=1-2$ THz we obtain $D^*\simeq(4.1-8.2)\times 10^8$ cm Hz$^{1/2}$/W. Setting $K=50$, we arrive at $D^*\simeq(1.7-3.4)\times 10^9$ cm Hz$^{1/2}$/W. Due to a significant decrease in the thermogeneration rate at lower temperatures, the detectivity markedly increases with decreasing temperature. Indeed, at $T=77$ K, setting $g_{\rm th}=10^{13}$ cm^{-2} s^{-1},[27] we obtain $D^*\simeq(1.7-3.4)\times 10^{13}$ cm Hz$^{1/2}$/W.

Figure 2 shows the dependences of the dc responsivity

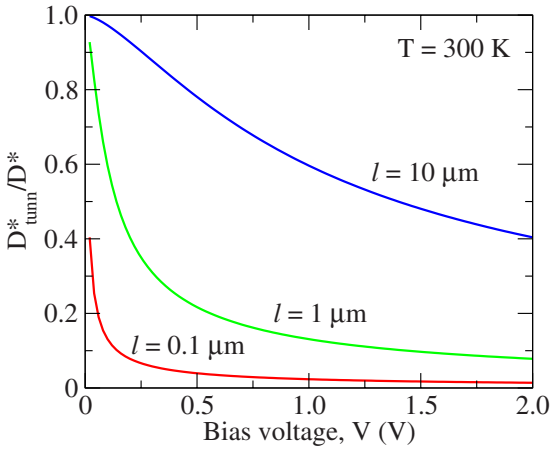

FIG. 3. (Color online) Normalized detectivity vs reverse bias voltage for GLDPs with different length of the i-section $2l$.

and detectivity on the number of GLs K calculated for $\Omega/2\pi=2$ and 3 THz using Eqs. (5) and (7) for GLPDs with sufficiently large l in which the tunneling is weak (see below). Equation (7) shows that the GLPD detectivity decreases with increasing photon frequency. This is because the spectral dependence of the GLPD detectivity is determined by that of the responsivity. As follows from Eqs. (6) and (7), the detectivity drops at elevated bias voltages when the interband tunneling prevails over the thermogeneration of the electron and hole pairs. According to Eqs. (4) and (7), the GLPD responsivity is independent of the length of the i-section $2l$ and the bias voltage V (at least if the latter is not too small), whereas the detectivity increases with increasing l and decreases with V. This is because the component of the dark current associated with the thermogeneration rate increases linearly with increasing l. At the same time, the tunneling component is proportional to $V^{3/2}/\sqrt{l}$. As a result, from Eq. (7) one can arrive at

$$D^* \propto \frac{1}{\sqrt{1+b(V/l)^{3/2}}}, \tag{8}$$

where $b \propto 1/g_{\rm th}$. Thus, at elevated bias voltages when the tunneling generation surpassed the thermal generation, $D^* \propto V^{-3/4}$. Figure 3 shows the voltage-dependence of the detectivity $D^*_{\rm tunn}$ with the interband tunneling normalized by the detectivity D^* without tunneling calculated for different values of the i-section length $2l$.

Since the value of D^* is determined by both l and V, the latter values should be properly chosen. There is also a limitation associated with the necessity to satisfy the condition $2l \lesssim l_R$, where l_R is the recombination length. Otherwise, the recombination in the i-section can become essential resulting in degrading of the GLPD performance. The recombination length can be defined as $l_R=L_V$, where $L_V \simeq \langle v\rangle \tau_R$, τ_R is the recombination time, and $\langle v\rangle$ is the average drift velocity in the i-region. Assuming that for the electron and hole densities close to that in the intrinsic graphene at $T=300$ K, one can put $\tau_R=5\times10^{-10}$ s. Setting for sufficiently large bias $\langle v\rangle=5\times10^7$ cm/s,[28] one can find $L_V \simeq 250$ μm.

III. FEATURES OF GLPD WITH ELECTRICALLY INDUCED JUNCTION

The main distinctions of the detectors with doped and electrically induced p-i-n junction are that the Fermi energies of electrons and holes in the latter depend on the gate voltages $V_p<0$ in the p-section and $V_n>0$ in the n-section [see Fig. 1(b)] and that these energies and, hence, the heights of the barriers confining electrons and holes in the pertinent section are different in different GLs. This is due to the screening of the transverse electric field created by the gate voltages by the GL charges. This screening results in a marked decrease in the barrier heights of the GLs located in the MGL-structure depth (with large indices k) in comparison with the GLs near the top. In the following, we set $V_n=-V_p=V_g$. The barriers in question effectively prevent the electron and hole injection from the contacts under the reverse bias if the barrier heights are sufficiently large. However, the electron and hole injection into the GLs with large k leads to a significant increase in the dark current (in addition to the current of the electrons and hole generated in the i-section). This can substantially deteriorate the GLPD detectivity. As for the responsivity, it can still be calculated using Eq. (4) or Eq. (5). To preserve sufficiently high detectivity, the number of GLs should not be too large. Indeed, taking into account the contributions of the current injected from the p- and n-regions to the net dark current, the detectivity of a GLPD with the electrically induced p-i-n junction can be presented as

$$D^* = \frac{K^*\beta_\Omega}{\hbar\Omega\sqrt{2\left[\Sigma_{k=1}^K j_i^{(k)}/el + K(g_{\rm th}+g_{\rm tunn})\right]}}, \tag{9}$$

where $j_i^{(k)} \propto \exp(-\varepsilon_F^{(k)}/k_BT)$ is the electron current injected from the p-region and the hole current injected from the n-region, and $\varepsilon_F^{(k)}$ is the Fermi energy of holes (electrons) in the p-region (n-region) of the kth GL ($1\le k\le K$).

The injected currents are small in comparison with the current of the electrons and holes thermogenerated in the i-region if

$$\frac{v_W\Sigma_0}{\pi}\exp\left(-\frac{\varepsilon_F^{(k)}}{k_BT}\right) < 2lg_{\rm th}. \tag{10}$$

Here Σ_0 is the electron and hole density in the intrinsic graphene (at given temperature).

Considering Eqs. (A5) and (A6) from the Appendix, the latter imposes the following limitation on the number of GLs in GLDs with the electrically induced p-i-n junctions and the gate voltage V_g:

$$K < K^{\rm max} = \frac{1}{\gamma}\sqrt{\frac{\varepsilon_F^T}{k_BT\ln(v_W\Sigma_0/2\pi lg_{\rm th})}} \propto V_g^{1/12}. \tag{11}$$

The quantity γ is defined in the Appendix. For $\gamma=0.12$, assuming that the Fermi energy in the topmost GL $\varepsilon_F^{(1)}=\varepsilon_F^T=100$ meV, $T=300$ K, $\Sigma_0 \simeq 8\times10^{10}$ cm^{-2}, $l=10$ μm, and $g_{\rm th}\simeq10^{21}$ cm^{-2} s^{-1}, we obtain $K^{\rm max}\simeq34$, i.e., fairly large. A decrease in l results in smaller $K^{\rm max}$ due to a substantial increase in the tunneling current. For instance, if $l=0.1$ μm,[11] we obtain $K^{\rm max}\simeq7$.

Thus, by applying gate voltages one can form the p- and n-sections with sufficiently high densities and large Fermi energies of holes and electrons in GL-structures with a large number of GLs.

IV. DYNAMICAL RESPONSE

To describe the dynamic response to the signals modulated with the frequency $\omega \ll \Omega$, one needs to find the ac components of the net density of photogenerated electron and holes, $\delta\Sigma_\omega^-$ and $\delta\Sigma_\omega^+$, respectively. These components are governed by the following equation:

$$-i\omega\delta\Sigma_\omega^{\mp} \pm \langle v\rangle \frac{d\delta\Sigma_\omega^{\mp}}{dx} = \sum_{k=1}^{K} \frac{\beta_\Omega \delta I_\omega^k}{\hbar\Omega}. \tag{12}$$

As in above, $\delta I_\omega^{(k)} = \delta I_\omega (1-\beta)^{K-k}$, so that

$$\sum_{k=1}^{K} \frac{\beta_\Omega \delta I_\omega^{(k)}}{\hbar\Omega} = K^* \frac{\beta_\Omega \delta I_\omega}{\hbar\Omega}.$$

In the case of ballistic transport of electrons and holes across the i-section, $\langle v\rangle \simeq v_W$. If the electron and hole transport is substantially affected by quasielastic scattering, so that the momentum distributions of electrons and holes are virtually semi-isotropic, one can put $\langle v\rangle \simeq v_W/2$ (see also Ref. 28). Solving Eq. (12) with the boundary conditions $\delta\Sigma_\omega^{\mp}|_{x=\pm l}=0$, we obtain

$$\delta\Sigma_\omega^{\mp} = K^* \frac{\beta_\Omega}{\hbar\Omega} \cdot \frac{\exp[i\omega(l \pm x)/\langle v\rangle] - 1}{i\omega} \delta I_\omega. \tag{13}$$

Using Eq. (13) and considering the Ramo–Shockley theorem[28,29] applied to the case of specific contact geometry[30] the ac current induced in the side contacts (terminal current) can be presented as

$$\frac{\delta I_\omega^{\text{photo}}}{\delta I_\omega} = K^* \frac{el\beta_\Omega}{\pi\hbar\Omega} \int_{-1}^{1} \frac{d\xi}{\sqrt{1-\xi^2}} \frac{[e^{i\omega\tau_t} \cos(\omega\tau_t\xi) - 1]}{i\omega\tau_t}. \tag{14}$$

Here we introduced the characteristic transit time $\tau_t = l/\langle v\rangle$. The feature of the contact geometry (the bladelike contacts) was accounted for by using the form factor $g(\xi) = 1/\pi\sqrt{1-\xi^2}$.[31] This is valid because the thickness of the side contacts and multiple-GL structure under consideration $Kd \ll l$ even at rather large numbers of GLs K, where d is the spacing between GLs. Similar approach was used previously to analyze the dynamic response of the lateral p-n junction photodiodes made of the standard semiconductors[32] and the graphene tunneling transit-time terahertz oscillator.[22] Integrating in Eq. (14), we arrive at the following:

$$\frac{\delta I_\omega^{\text{photo}}}{\delta I_\omega} = K^* \frac{4el\beta_\Omega}{\hbar\Omega} \left[\frac{\sin(\omega\tau_t)\mathcal{J}_0(\omega\tau_t)}{\omega\tau_t} + i\frac{1-\cos(\omega\tau_t)\mathcal{J}_0(\omega\tau_t)}{\omega\tau_t} \right], \tag{15}$$

where $\mathcal{J}_0(\xi)$ is the Bessel function. Equation (15) yields

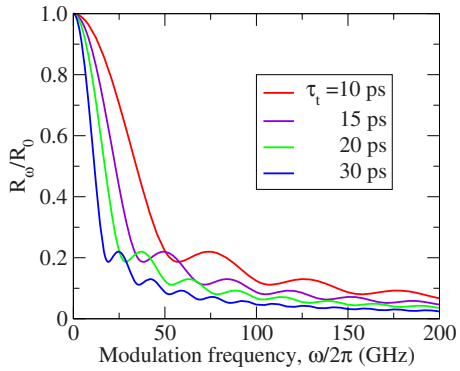

FIG. 4. (Color online) Dependence of responsivity (normalized) on modulation frequency $\omega/2\pi$ for different τ_t.

$$\frac{|\delta I_\omega^{\text{photo}}|}{\delta I_\omega} = K^* \frac{4el\beta_\Omega}{\hbar\Omega} \frac{\sqrt{1-2\cos(\omega\tau_t)\mathcal{J}_0(\omega\tau_t) + \mathcal{J}_0^2(\omega\tau_t)}}{\omega\tau_t}. \tag{16}$$

Using Eq. (16), for the frequency dependent responsivity $R_\omega = |\delta I_\omega^{\text{photo}}|/2l\delta I_\omega$, we obtain

$$R_\omega = K^* \frac{2e\beta}{\hbar\Omega} \frac{\sqrt{1-2\cos(\omega\tau_t)\mathcal{J}_0(\omega\tau_t) + \mathcal{J}_0^2(\omega\tau_t)}}{\omega\tau_t} = R_0 \frac{\sqrt{1-2\cos(\omega\tau_t)\mathcal{J}_0(\omega\tau_t) + \mathcal{J}_0^2(\omega\tau_t)}}{\omega\tau_t}. \tag{17}$$

Figure 4 shows the responsivity R_ω normalized by its dc value versus the modulation frequency ω calculated using Eq. (17) for different values of the transit time $\tau_t \propto l$. At $\langle v\rangle = v_W/2 \simeq 5\times 10^7$ cm/s, the range $\tau_t = 10-30$ ps corresponds to the length of the i-section $2l = 10-30$ μm. As seen from Fig. 4, $R_\omega/R_0 = 1/\sqrt{2}$ when the modulation cutoff frequency $f_t = \omega_t/2\pi \simeq 8.3-24.9$ GHz. Naturally, in GLPDs with shorter i-sections, f_t can be markedly larger (although, at the expense of a substantial increase in the tunneling current). Due to this, GLPDs can be used as ultrafast terahertz and IR photodetectors (Fig. 4).

V. COMPARISON WITH QWIPS AND QDIPS

Now we compare the responsivity and detectivity of GLPDs with K GLs calculated above and those of QWIPs (properly coupled with the incident terahertz or IR radiation) and QDIPs with the same number of QWs. The fraction of the absorbed photon flux in one QW $\beta_\Omega^{(\text{QW})} \simeq \sigma_\Omega^{(\text{QW})}\Sigma_0^{(\text{QW})}$, where $\sigma^{(\text{QW})}$ is the cross section of the photon absorption due to the intersubband transitions and Σ_d the donor sheet density. Setting the usual values $\sigma_\Omega^{(\text{QW})} \simeq 2\times 10^{-15}$ cm^2 and $\Sigma_O^{(\text{QW})} \simeq 10^{12}$ cm^{-2}, one obtains $\beta_\Omega^{(\text{QW})} \simeq 0.002$. This value is one order of magnitude smaller that β_Ω. Hence, one can neglect the attenuation of radiation in QWIPs with $K \lesssim 100$ (whereas in GLPDs it can be essential). In such a case, the responsivity of QWIPs is independent of the number of QWs K in the QWIP structure[33] and given by

$$R_0^{(\mathrm{QW})} = \frac{e\beta_\Omega^{(\mathrm{QW})}}{\hbar\Omega p_c}, \tag{18}$$

where p_c is the so-called capture probability which relates to the QWIP gain $G^{(\mathrm{QW})}$ as $G^{(\mathrm{QW})}=(1-p_c)/Kp_c \simeq 1/Kp_c$.[33] Using Eqs. (4) and (18), we obtain

$$\frac{R_0}{R_0^{(\mathrm{QW})}} \simeq \frac{2\beta_\Omega p_c}{\beta_\Omega^{(\mathrm{QW})}} K^*. \tag{19}$$

Assuming that $K=50-100$, ($K^* \simeq 30-39$), $\beta_\Omega^{(\mathrm{QW})}=0.002$, and $p_c=0.1$, we obtain $R_0/R_0^{(\mathrm{QW})} \simeq 70-90$.

The ratio of the detectivities can be presented as

$$\frac{D^*}{D^{*(\mathrm{QW})}} \simeq \frac{2\beta_\Omega\sqrt{p_c}}{\beta_\Omega^{(\mathrm{QW})}} \frac{K^*}{K} \sqrt{\frac{g_{\mathrm{th}}^{(\mathrm{QW})}}{g_{\mathrm{th}}}}. \tag{20}$$

As can be extracted from Ref. 26, $g_{\mathrm{th}} \propto \exp(-\hbar\omega_0/k_BT)$, where $\hbar\omega_0 \simeq 0.02$ eV is the energy of optical phonon in GLs, whereas $g_{\mathrm{th}}^{(\mathrm{QW})} \propto \exp(-\varepsilon^{(\mathrm{QW})}/k_BT)$, where $\varepsilon^{(\mathrm{QW})}$ is the QW ionization energy ($\hbar\Omega \gtrsim \varepsilon^{(\mathrm{QW})}$), Eq. (17) yields

$$\frac{D^*}{D^{*(\mathrm{QW})}} \propto \frac{2\beta_\Omega\sqrt{p_c}}{\beta_\Omega^{(\mathrm{QW})}} \frac{K^*}{K} \exp\left[\frac{\hbar(\omega_0-\Omega)}{2k_BT}\right]. \tag{21}$$

Different dependences of the responsivities and detectivities of GLDs and QWIPs on K are due different directions of the dark current and photocurrent: parallel to the GL plane in the former case and perpendicular to the QW plane in the latter case. The product of the factors in the right-hand side of Eq. (21) except the last one can be on the order of unity. This is because a large ratio $2\beta_\Omega/\beta_\Omega^{(\mathrm{QW})}$ can be compensated by relatively small capture parameter p_c. However, the exponential factor in Eq. (21) is large in the terahertz range: $\Omega \lesssim \omega_0$, i.e., at $\Omega/2\pi \lesssim 50$ THz. In particular, at $T=300$ K and $\Omega/2\pi=5-10$ THz, the exponential factor in question is about 24–36.

The GLPD responsivity and detectivity can also markedly exceed those of QDIPs [for which formulas similar to Eqs. (21) can be used] despite lower capture probability and thermoexcitation rate in QDIPs in comparison with QWIPs (see, for instance, Refs. 34–36). The ratios $D^*/D^{*(\mathrm{QW})}$ and $D^*/D^{*(\mathrm{QD})}$ dramatically increases with decreasing $\hbar\Omega$ and T. This is attributed to the fact that the spectral dependence of the GLPDs detectivity is similar to the spectral dependence of the responsivity ($D^* \propto \beta_\Omega/\hbar\Omega$), whereas the GLPDs intended for the photodetection in different spectral ranges exhibit the same dark current (due to the gapless energy spectrum). In contrast, in QWIPs, QDIPs, and some other photodetectors (see, for example, Refs. 9 and 10) the transition to lower photon frequency requires to utilize the structures with lower ionization energy and, hence, exponentially higher dark current. The latter leads to quite different spectral dependencies of the GLPD detectivity and the detectivity of QWIPs and QDIPs (which drops with creasing photon frequency).

GLPDs can surpass QWIPs and QDIPs in responsivity even at relatively high photon frequencies. For example, for a GLPD with $K=25$ at $\Omega/2\pi=75$ THz (wavelength λ about 4 μm), we arrive at $R_0 \simeq 3$ A/W. This value is three times larger than $R_0^{(\mathrm{QD})}$ obtained experimentally for a QDIP with 25 InAs QD layers.[37] As for the detectivity, comparing a GLPD with $K=70$ operating at $T=300$ K and $\Omega/2\pi \simeq 15$ THz ($\lambda \simeq 20$ μm) and a QDIP with 70 QD layers,[38] we obtain $D^* \sim 2\times 10^8$ cm Hz$^{1/2}$/W and $D^{*(\mathrm{QD})} \sim 10^7$ cm Hz$^{1/2}$/W, respectively.

GLPDs can surpass also photodetectors on narrow-gap and gapless bulk semiconductors like HgCdTe (BSPDs). Apart from advantages associated with potentially simpler fabrication, GLPDs might exhibit higher detectivity (compare the data above and those from Ref. 39). This can be attributed to relatively low thermogeneration rate in GLPDs compared to BSPDs with very narrow or zeroth gap. The point is that thermogeneration rate in GLPDs at room temperatures is primarily due absorption of optical phonons[27] which have fairly large energy $\hbar\omega_0$ (the Auger processes in GLs are forbidden),[40] whereas this rate in BSPDs is essentially determined by the Auger processes which are strong.[39]

VI. DISCUSSION AND CONCLUSIONS

Analyzing Eqs. (4)–(7), we accepted that $f(\hbar\Omega) \ll 1$ and, therefore, disregarded the frequency dependence of the absorption coefficient β_Ω associated with the population of the low energy states by electrons and holes. For a rough estimate, the value of distribution function $f(0)$ can be presented as $f(0) \lesssim f_0(0)\Sigma/\Sigma_0$, where Σ is the electron and hole density in the i-section under the reverse bias. This density, in turn, can be estimated as $\Sigma=2g_{\mathrm{th}}\tau_t=g_{\mathrm{th}}2l/\langle v\rangle$. Using the same parameters as above, for $l=10$ μm and $T=30$ K, we obtain $\Sigma/\Sigma_0=0.25$, so that $f(0) \lesssim 0.125$ and $\beta_\Omega|_{\Omega\to 0} \gtrsim 0.75\beta$. It implies that the numerical data obtained above for the frequencies at the lower end of the terahertz range might be slightly overestimated. However, since the electron-hole system in the i-section can be pronouncedly heated by the electric field, the actual values of $f(\hbar\Omega/2)$ can be smaller than in the latter estimate and, hence, β_Ω can be rather close to β. The electron and hole heating in intrinsic GLs under the electric field was studied recently.[28,41] As shown in Ref. 41 solving the kinetic equations, the electron and hole distribution functions in a GL in the range of low energies becomes $f(0)$ become small at fairly small electric fields. Indeed, at $T=300$ K, $f(0)$ varies from $f(0) \simeq 0.2$ to $f(0) \simeq 0.05$ when the electric field E increases from $E=3$ V/cm to $E=30$ V/cm. For a GLPD with the length of the i-section $2l=10-30$ μm (as in the estimates in Secs. III and IV), these values of the electric field correspond to the reverse bias voltage $V \simeq 3\times 10^{-3}-9\times 10^{-2}$ V. Hence, the electron and hole populations in the i-section should not lead to a marked deviation of the GL absorption β_Ω from β=const. In contrast with the cases considered in Refs. 28 and 41, The finiteness of the transit time of electrons and holes in the i-section of the GL-structures under consideration might affect the electron and hole heating resulting in minor modification of the absorption coefficient. Therefore, more careful calculation of β_Ω at relatively low Ω can, in principle, be useful.

In summary, we proposed and evaluated GLPDs based multiple-GL p-i-n structures. It was shown that GLPDs can

exhibit high responsivity and detectivity in the terahertz and IR ranges at room temperatures. Due to relatively high quantum efficiency and low thermogeneration rate, the GLPD responsivity and detectivity can substantially exceed those of other photodetectors.

ACKNOWLEDGMENTS

The authors are grateful to M. S. Shur, A. A. Dubinov, V. V. Popov, A. Satou, M. Suemitsu, and F. T. Vasko for fruitful discussions and comments. This work was supported by the Japan Science and Technology Agency, CREST, Japan.

APPENDIX: EFFECT OF VERTICAL SCREENING IN MULTIPLE GL-STRUCTURES

As was pointed out above, the thickness of multiple GL-structures even with rather large number of GLs K is in reality small in comparison with the lateral sizes of the device, namely, the lengths of all the section and, hence, the gates. Owing to this, the distribution of the dc electric potential $\psi=2\varphi_0/V_g$ normalized by $V_g/2$ (where $V_g=V_n=-V_p$) in the direction perpendicular to the GL plane (corresponding to the axis z) can be found from the one-dimensional Poisson equation:

$$\frac{d^2\psi}{dz^2}=\frac{8\pi e}{\varkappa V_g}\sum_{k=1}^{K}\Sigma^{(k)}\delta(z-kd+d). \tag{A1}$$

Here $\Sigma_0^{(k)}$ is the electron (hole) density in the kth GL in the n-section (p-section), d is the spacing between GLs, and $\delta(z)$ is the Dirac delta function. Considering that $\Sigma_0^{(k)}=(\varepsilon_F^k)^2/\pi\hbar^2v_F^2=(e^2V_g^2/4\pi\hbar^2v_F^2)\psi^2|_{z=kd}$, where ε_F^k is the Fermi energy in the n-section (p-section) of the kth GL, and replacing the summation in Eq. (A1) by integration (that is valid if K is not too small), we reduce Eq. (A1) to the following:

$$\frac{d^2\psi}{dz^2}=\frac{\psi^2}{L_s^2}, \tag{A2}$$

with the characteristic screening length $L_s=\hbar v_F\sqrt{\varkappa d/2e^3V_g}\propto V_g^{-1/2}$. One can assume that $\psi|_{z=0}=2+W_g(d\psi/dz)|_{z=0}$ and $\psi|_{z=\infty}=0$ [as well as $(d\psi/dz)|_{z=\infty}=0$], where W_g is the thickness of the layer separating the multiple GL-structure and the gates. Solving Eq. (A2) with the latter boundary conditions, we arrive at

$$\psi=\frac{1}{(C+z/\sqrt{6}L_s)^2}, \tag{A3}$$

where C satisfies the following equation:

$$C^3-C/2=(W_g/\sqrt{6}L_s). \tag{A4}$$

Since in reality $W_g\gg\sqrt{6}L_s$, one obtains $C\simeq(W_g/\sqrt{6}L_s)^{1/3}\propto V_g^{1/6}$. Setting $d=0.35$ nm, $W_g=10$ nm, $\varkappa=4$, and $V_g=2$ V, one can obtain $L_s\simeq0.31$ nm, and $C\simeq2.4$.

Equation (A3) yields

$$\varepsilon_F^{(k)}\simeq\frac{eV_g}{2[C+(k-1)d/\sqrt{6}L_s]^2}=\varepsilon_F^Ta^{(k)}. \tag{A5}$$

Here $\varepsilon_F^T=\varepsilon_F^{(1)}=eV_g/2C^2\propto(V_g/W_g)^{2/3}$ is the Fermi energy of electrons in the topmost GL in the n-section (holes in the p-section) and

$$a^{(k)}=[1+(k-1)\gamma]^{-2}, \tag{A6}$$

where $\gamma=d/\sqrt{6}L_sC\propto V_g^{1/3}$. At the above parameters (in particular, $W_g=10-50$ nm and $V_g=2$ V) $\gamma=d/\sqrt{6}L_sC\simeq0.12-0.20$.

[1] C. Berger, Z. Song, T. Li, X. Li, A. Y. Ogbazhi, R. Feng, Z. Dai, A. N. Marchenkov, E. H. Conrad, P. N. First, and W. A. de Heer, J. Phys. Chem. **108**, 19912 (2004).
[2] K. S. Novoselov, A. K. Geim, S. V. Morozov, D. Jiang, M. I. Katsnelson, I. V. Grigorieva, S. V. Dubonos, and A. A. Firsov, Nature (London) **438**, 197 (2005).
[3] A. H. Castro Neto, F. Guinea, N. M. R. Peres, K. S. Novoselov, and A. K. Geim, Rev. Mod. Phys. **81**, 109 (2009).
[4] F. T. Vasko and V. Ryzhii, Phys. Rev. B **77**, 195433 (2008).
[5] V. Ryzhii, M. Ryzhii, and T. Otsuji, J. Appl. Phys. **101**, 083114 (2007).
[6] F. Rana, IEEE Trans. Nanotechnol. **7**, 91 (2008).
[7] A. Satou, F. T. Vasko, and V. Ryzhii, Phys. Rev. B **78**, 115431 (2008).
[8] A. A. Dubinov, V. Ya. Aleshkin, M. Ryzhii, T. Otsuji, and V. Ryzhii, Appl. Phys. Express **2**, 092301 (2009).
[9] V. Ryzhii, V. Mitin, M. Ryzhii, N. Ryabova, and T. Otsuji, Appl. Phys. Express **1**, 063002 (2008).
[10] V. Ryzhii and M. Ryzhii, Phys. Rev. B **79**, 245311 (2009).
[11] F. Xia, T. Murller, Y.-M. Lin, A. Valdes-Garsia, and F. Avouris, Nat. Nanotechnol. **4**, 839 (2009).
[12] P. Neugebauer, M. Orlita, C. Faugeras, A.-L. Barra, and M. Potemski, Phys. Rev. Lett. **103**, 136403 (2009).
[13] V. Ryzhii, M. Ryzhii, A. Satou, T. Otsuji, A. A. Dubinov, and V. Ya. Aleshkin, J. Appl. Phys. **106**, 084507 (2009).
[14] Yu.-M. Lin, D. B. Farmer, G. S. Tulevski, S. Xu, R. G. Gordon, and P. Avouris, Device Research Conf., Tech. Dig., p. 27 (2008).
[15] D. Wei, Y. Liu, Y. Wang, H. Zhang, L. Huang, and G. Yu, Nano Lett. **9**, 1752 (2009).
[16] J. Zhu and J. C. S. Woo, Ext. Abstracts of the 2009 Int. Conf. on Solid State Devices and Materials, Sendai, 2009 (unpublished), pp. G-9–G-2.
[17] V. V. Cheianov and V. I. Fal'ko, Phys. Rev. B **74**, 041403(R) (2006)
[18] L. M. Zhang and M. M. Fogler, Phys. Rev. Lett. **100**, 116804 (2008).
[19] B. Huard, J. A. Sulpizio, N. Stander, K. Todd, B. Yang, and D. Goldhaber-Gordon, Phys. Rev. Lett. **98**, 236803 (2007).
[20] B. Özyilmaz, P. Jarillo-Herrero, D. Efetov, D. Abanin, L. S. Levitov, and P. Kim, Phys. Rev. Lett. **99**, 166804 (2007).
[21] M. Ryzhii and V. Ryzhii, Jpn. J. Appl. Phys., Part 2 **46**, L151 (2007).
[22] V. Ryzhii, M. Ryzhii, V. Mitin, and M. S. Shur, Appl. Phys. Express **2**, 034503 (2009).
[23] A. Bostwick, T. Ohta, T. Seyller, K. Horn, and E. Rotenberg, Nat. Phys. **3**, 36 (2007).
[24] L. A. Falkovsky and A. A. Varlamov, Eur. Phys. J. B **56**, 281 (2007).
[25] A. Rose, *Concepts in Photoconductivity and Allied Problems* (Wiley, New York, 1963).
[26] *Long Wavelength Infrared Detectors*, edited by M. Razeghi (Gordon and Breach, Amsterdam, 1996).
[27] F. Rana, P. A. George, J. H. Strait, S. Shivaraman, M. Chanrashekhar, and M. G. Spencer, Phys. Rev. B **79**, 115447 (2009).
[28] R. S. Shishir, D. K. Ferry, and S. M. Goodnick, J. Phys.: Conf. Ser **193**, 012118 (2009).
[29] S. Ramo, Proc. IRE **27**, 584 (1939).
[30] C. K. Jen, Proc. IRE **29**, 345 (1941).
[31] V. Ryzhii and G. Khrenov, IEEE Trans. Electron Devices **42**, 166 (1995).
[32] N. Tsutsui, V. Ryzhii, I. Khmyrova, P. O. Vaccaro, H. Taniyama, and T. Aida, IEEE J. Quantum Electron. **37**, 830 (2001).
[33] H. Schneider and H. C. Liu, *Quantum Well Infrared Photodetectors* (Springer, Berlin, 2007).
[34] V. Ryzhii, Semicond. Sci. Technol. **11**, 759 (1996).
[35] V. Ryzhii, I. Khmyrova, M. Ryzhii, and V. Mitin, Semicond. Sci. Technol. **19**, 8 (2004).

[36]A. Rogalski, J. Antoszewski, and L. Faraone, J. Appl. Phys. **105**, 091101 (2009).
[37]H. Lim, S. Tsao, W. Zhang, and M. Razeghi, Appl. Phys. Lett. **90**, 131112 (2007).
[38]S. Chakrabarti, A. D. Siff-Roberts, X. H. Su, P. Bhattacharya, G. Ariyawansa, and A. G. U. Perera, J. Phys. D **38**, 2135 (2005).
[39]P. Martyniuk, S. Krishna, and A. Rogalski, J. Appl. Phys. **104**, 034314 (2008).
[40]M. S. Foster and I. L. Aleiner, Phys. Rev. B **79**, 085415 (2009).
[41]O. G. Balev, F. T. Vasko, and V. Ryzhii, Phys. Rev. B **79**, 165432 (2009).